Anisotropic quark stars with an interacting quark equation of state

E. A. Becerra-Vergara,[1,2,3,*] Sindy Mojica,[1,†] F. D. Lora-Clavijo,[1,‡] and Alejandro Cruz-Osorio[4,5,§]

[1]*Grupo de Investigación en Relatividad y Gravitación, Escuela de Física, Universidad Industrial de Santander A. A. 678, Bucaramanga 680002, Colombia*

[2]*Dipartimento di Fisica, Sapienza Università di Roma, P.le Aldo Moro 5, I–00185 Rome, Italy*

[3]*ICRANet, Piazza della Repubblica 10, I–65122 Pescara, Italy*

[4]*Departamento de Astronomía y Astrofísica, Universitat de Valéncia, Dr. Moliner 50, 46100, Burjassot (Valéncia), Spain*

[5]*Institut für Theoretische Physik, Max-von-Laue-Straße 1, 60438 Frankfurt, Germany*

(Received 11 March 2019; revised manuscript received 10 July 2019; published 11 November 2019)

A deep exploration of the parameter space that relates the interacting equation of state with the bag constant B, and the interaction parameter a, is fundamental for the construction of diverse models of quark stars. In particular, the anisotropy of quark stars with a well-motivated quantum chromodynamics (QCD) equation of state is presented here. The contribution of the fourth order corrections parameter (a_4) of the QCD perturbation on the radial and tangential pressure generate significant effects on the mass-radius relation and the stability of the quark star. An adequate set of solutions for several values of the bag factor and the interaction parameter are used in order to calculate the relation between the mass, radius, density, compactness, and consequently the maximum masses and the stability. Therefore, while the more interactive quark solution leads to higher masses, the weak interaction among quarks gives solutions similar to the widely known MIT bag model.

DOI: 10.1103/PhysRevD.100.103006

I. INTRODUCTION

Anisotropy of compact objects [1,2] is one of the main topics that have been studied in several astrophysical systems like boson stars [3], gravastars [4] and neutron stars [5]. Essentially, the anisotropy is presented as the difference between the radial and the tangential pressure $(P - P_\perp)$ in the hydrostatic equilibrium equation which is obtained solving the Einstein field equations for the interior of the star.

The ongoing knowledge about anisotropy could not have been possible without the statements settled by previous studies. For example, Ruderman [6] theoretically showed that anisotropic effects could arise in stellar models, where nuclear matter reaches densities larger than 10^{15} g/cm^3 due to the interactions that at this level are relativistic. Likewise, phase transitions [7,8] between the inner core and the outer crust occur when the matter goes to a superfluid and superconductive state, generating significant changes in the interior of a star. Also, the pion phase configuration [1,9], and solid state configurations at densities of 10^{14}–10^{15} orders of magnitude [10,11], and in other cases strong magnetic fields [12,13] may produce anisotropies with observable consequences. These and other mechanisms producing anisotropies can be found in [14], and in the recent publication [1].

In order to measure the possible anisotropic effects, compact objects like neutron stars are taken as astrophysical laboratories to check how they are affected by this phenomenon. In a pioneering work by Bowers and Liang [15], the Einstein field equations for anisotropic spheres and incompressible matter were solved, and the effects of the anisotropy in the resulting maximum mass and red shift were discussed. Afterwards, Cosenza *et al.* [16] presented a set of solutions with anisotropic sources based on known solutions for an isotropic matter. Later, numerical solutions [2] exhibited a good agreement with the mass-radius relations, but also calculated the upper limit mass of a stable neutron star by taking an arbitrarily high value of the anisotropy [5].

Motivated by the current achievements in order to understand the processes that produce anisotropies, and the advances in nuclear physics that have shown the behavior of matter in the outer layers of a neutron star interior at certain densities, and in spite of the lack of knowledge about matter interactions at higher densities than the saturation nuclear matter density value, many theories have suggested that the neutron star core has *exotic* [17] constituents like hyperons, kaon condensates, or a deconfined phase of strange matter. Other theories suggest [18] the existence of hybrid stars made of hadronic matter

*eduar.becerra@icranet.org
†sindroc@gmail.com
‡fadulora@uis.edu.co
§osorio@th.physik.uni-frankfurt.de

mixed with quarks and a core purely made of quarks. However, quark stars (QS) can be generated by different processes, for instance, a core collapse after a supernova explosion [19], where the conversion of ordinary matter to quark matter in a deconfined core [20,21] takes place. Other theories advocate for phase transitions that occur as consequence of the mass accretion in a low mass x-ray binary system [22]. Therefore, there is no reason to ignore the existence of another type of compact objects apart from neutron stars.

The usual equation of state (EOS) utilized to obtain solutions for quark stars is the well-known MIT bag model [23,24] since it seems to be adequate to describe the behavior of matter that is not governed by gravity but instead by the strong nuclear force. However, this EOS is not sufficiently powerful to characterize a system with interacting quarks or more complex structures. It is to expect that interactions among quarks must generate changes at the interior of the shell generating anisotropies that change the mass-radius relation and the gravitational redshift. Therefore, this also suggests that the equation of state can be constrained by considering the anisotropies at its interior produced by the mechanisms previously mentioned. So, in order to model anisotropic quark stars, several methods have been proposed. In [25], the anisotropy is modeled by taking two different expressions for the pressure; while the radial pressure is written as a lineal EOS, the tangential pressure is taken as a complex expression dependent on the radial coordinate. As a result this model yields to a mass-radius relation that exhibits values up to 3 $M_{\odot}$. On the other hand, a different approach given by a deterministic model [20] used the MIT bag EOS; for this case observational evidence that contemplates the existence of strange stars is considered in order to make an interpolation function of the mass $m(r)$, where the obtained solutions are in agreement with Buchdahl model, which is explained with more detail in [26]. Another complementary work for the anisotropy of nonrotating strange stars and its effect in the usual physical observables is calculated in [27]; its aim is to test the stability of the model with a generalization of the Tolman-Oppenheimer-Volkoff (TOV) equation using the Herrera's cracking concept [28]. Meanwhile, other models are focused on the attempt to find a singularity-free solution of the Einstein equations [29,30] through the MIT bag model to obtain the mass-radius relation for different values of the bag constant. Additionally, in [29] the authors took the density profile given in [25] and addressed their computations to obtain the total mass of the quark star. In this case, a general expression for the TOV equation was calculated; the stability of the system was evaluated with the Herrera's cracking concept, while the energy condition was satisfied. Another method [30] suggested a new model that uses the homotopy perturbation method, in order to find a solution for spherically symmetric quark stars whose results were compared with quark star candidates like *CenX-3*, *VelaX-1* [31], $4U1820-30$ [32], $J1903+0327$ [33], $4U1820-30$ [34], and $PSRJ1614-2230$ [35].

It is clear that following the current knowledge on the neutron stars and their layers, one should not discard the existence of more exotic objects, and although compact objects appear to be isotropic and homogeneous from the observations, it is impossible to think that their interiors are perfectly arranged to be considered as isotropic, since the nuclear phenomena that occur in the crust and the core are highly intense, generating anisotropies and consequently producing changes on the mass-radius relation, as we see henceforth. In Sec. II a QCD motivated EOS is introduced and the Tolman-Oppenheimer-Volkoff equations are obtained. In Sec. III the numerical details to obtain the mass-radius relation and the full set of solutions presented in Secs. IV and V are explained. Finally, the highlight results and further research are proposed in Sec. VI.

II. THE MODEL

A. Quark matter equation of state

In spite of the fact that strange stars have not been directly observed yet, there are some candidates [17,36,37] that could fit the EOS associated with this type of object. Those candidates seem not to adjust their masses and radius to the neutron stars models, but by means of a semiempirical relation that calculates the strength of the magnetic field of a pulsar [37], a range for the mass-radius relation is obtained giving a good description of strange star composers. A widely accepted quark star model is the MIT bag model that characterizes a degenerated Fermi gas of quarks up, down and strange [23,24,38,39]. This is the simplest and more frequently used form to illustrate the interior as a quark star [23]. Nevertheless, quark stars are not such simple objects that only depend on the bag constant B; indeed, this led to the construction of several models based on quantum chromodynamics (QCD) corrections of second and fourth order with the aim of giving an approximate characterization of confined quarks, like that presented in [40]. This model not only includes the interactions among quarks, but also suggests the possibility of the existence of new matter states analogous to the superconductivity state Bardeen, Cooper, and Schrieffer (BCS), that is, a phase known as the colour flavor locked phase (CFL).

Following the EOS mentioned above [40], we consider homogeneously confined matter inside the star with three-flavor neutral charge and a fixed strange quark mass m_s. But for simplicity, the superconductivity generated in the CFL phase is not taken into account; thus the EOS reduces to the expression [41]

$$P=\frac{1}{3}(\epsilon-4B)-\frac{m_s^2}{3\pi}\sqrt{\frac{\epsilon-B}{\mathrm{a}_4}}+\frac{m_s^4}{12\pi^2}\left[1-\frac{1}{\mathrm{a}_4}+3\ln\left(\frac{8\pi}{3m_s^2}\sqrt{\frac{\epsilon-B}{\mathrm{a}_4}}\right)\right], \quad (1)$$

where ϵ is the energy density of the homogeneously distributed quark matter, the quark strange mass is $m_s = 100$ MeV [42], and B is the bag constant whose values run between $B > 57$ MeV/fm^3 and $B < 92$ MeV/fm^3, which are determined by the stability condition with respect to iron nuclei for two-flavor and the three-flavor quark matter respectively. This implies that strange quark matter is absolutely stable for a range of energy densities of $57 < B < 92$ MeV/fm^3 [38]. Finally, a_4 is the parameter that comes from the QCD corrections on the pressure of the quark-free Fermi sea; this parameter is related to the maximum mass of the star with values of $\approx 2\,M_\odot$ for $\mathrm{a}_4 \approx 0.7$ [43].

B. Tolman-Oppenheimer-Volkoff equations

Let us consider an anisotropic fluid and a spherically symmetric spacetime, whose line element is given in terms of the components of the metric $g_{\alpha\beta}$ by

$$\mathrm{d}s^2=-c^2\alpha^2\mathrm{d}t^2+\left(1-\frac{2Gm}{c^2r}\right)^{-1}\mathrm{d}r^2+r^2\mathrm{d}\Omega, \quad (2)$$

where $\alpha=\alpha(r)$, $m=m(r)$, $\mathrm{d}\Omega=\mathrm{d}\theta^2+\sin^2\theta\mathrm{d}\phi^2$, G is the gravitational constant and c is the speed of light. The energy momentum tensor can be written as [44,45]

$$T_{\alpha\beta}=(\epsilon+P_\perp)u_\alpha u_\beta+P_\perp g_{\alpha\beta}+(P-P_\perp)n_\alpha n_\beta, \quad (3)$$

where P is the radial pressure and $P_\perp$ is the tangential pressure. We propose a new generalized EOS for the tangential pressure

$$P_\perp=P_c+\frac{1}{3}(\epsilon-4B_\perp)-\frac{m_s^2}{3\pi}\sqrt{\frac{\epsilon-B_\perp}{\mathrm{a}_4^\perp}}+\frac{m_s^4}{12\pi^2}\left[1-\frac{1}{\mathrm{a}_4^\perp}+3\ln\left(\frac{8\pi}{3m_s^2}\sqrt{\frac{\epsilon-B_\perp}{\mathrm{a}_4^\perp}}\right)\right]-\frac{1}{3}(\epsilon_c-4B_\perp)+\frac{m_s^2}{3\pi}\sqrt{\frac{\epsilon_c-B_\perp}{\mathrm{a}_4^\perp}}-\frac{m_s^4}{12\pi^2}\left[1-\frac{1}{\mathrm{a}_4^\perp}+3\ln\left(\frac{8\pi}{3m_s^2}\sqrt{\frac{\epsilon_c-B_\perp}{\mathrm{a}_4^\perp}}\right)\right], \quad (4)$$

with P_c and ϵ_c being the radial pressure (1) and the energy density, respectively, at the center of the star. From this expression it can be seen that the radial and tangential pressures are the same at $r=0$, i.e., when $B_\perp = B$ and $\mathrm{a}_4^\perp = \mathrm{a}$ this yields to $P_\perp = P_c$, which represents the case of an isotropic fluid. This also is a condition satisfied by the central energy density and the energy density at the center. Meanwhile for the rest of the star, as it can be inferred from the Tolman-Oppenheimer-Volkoff equation, if the tangential and the radial pressure are equal, the expression corresponding to the pressure will have contributions only from the first term. It is worth mentioning that $B_\perp$ and $\mathrm{a}_4^\perp$ parameters are the contributions on the tangential component of the pressure, and run in the same range of values as B and a_4.

On the other hand, $u^\alpha u_\alpha = -1$ and $n^\alpha n_\alpha = 1$ such that

$$u^\alpha=\left[\frac{1}{c\alpha},0,0,0\right], \quad (5)$$

$$n^\alpha=\left[0,\left(1-\frac{2Gm}{c^2r}\right)^{1/2},0,0\right]. \quad (6)$$

By solving the Einstein field equations and matter equations, a general expression for an anisotropic spherically symmetric compact star is obtained,

$$\frac{\mathrm{d}m}{\mathrm{d}r}=4\pi r^2\epsilon, \quad (7)$$

$$\frac{\mathrm{d}P}{\mathrm{d}r}=-\frac{(\epsilon+\frac{P}{c^2})(m+\frac{4\pi r^3P}{c^2})}{\frac{r^2}{G}(1-\frac{2Gm}{rc^2})}-\frac{2}{r}(P-P_\perp), \quad (8)$$

$$\frac{1}{\alpha}\frac{\mathrm{d}\alpha}{\mathrm{d}r}=\frac{G}{c^2r^2}\left(m+\frac{4\pi r^3P}{c^2}\right)\left(1-\frac{2Gm}{rc^2}\right)^{-1}. \quad (9)$$

Notice that the Eq. (8) is the only one that contains the contribution of the radial and tangential pressure by the difference $P-P_\perp$.

III. NUMERICAL DETAILS

The numerical calculations presented in this paper were carried out by using the CAFE astrophysical code [46]. All the simulations are computed using a fourth order Runge-Kutta integrator in a one-dimensional spherical grid, which extends from $r=0$ to the outer domain boundary, $r_{\max}=100$. It is worth mentioning that for all the models here considered the radii of the stars are inside $r_{\max}$. In all the simulations presented, we use a uniform spatial grid with spatial resolution $\Delta r = 0.01$. In order to avoid the singular behavior at $r=0$, we follow the procedure shown in [47], in which a Taylor expansion is made around this point. The resulting approximate regular equations are programmed for at least the first mesh point located at $r=\Delta r$, being Δr the uniform spatial resolution of the grid. On the other hand, the radius R of the surface of the star is

defined as the radius $r = R$, where the pressure $P(R) = 1 \times 10^{-30}$ which is an adimensional value.

Finally, for calculating the maximum masses and their corresponding radii, we have solved the TOV equations for several values of $a_4^\perp$ and $B_\perp$. Specifically the values of $a_4^\perp$ range from $a_4^\perp = 0.07$ to $a_4^\perp = 1$ with an interval of 0.0092, while the values of $B_\perp$ from $B = B_\perp = 57$ MeV/fm^3 to $B = B_\perp = 92$ MeV/fm^3 with an interval of 0.35. For each couple of fixed $a_4^\perp$ and $B_\perp$ we vary the central energy density from $1.7\epsilon_n$ to $3.3\epsilon_n$ with an interval of $0.003\epsilon_n$, being $\epsilon_n = 2.4 \times 10^{14}$ g/cm^3. These density values guarantee the typical central pressures of quark star candidates; for example, if the central pressure is calculated for $B = 57$ MeV/fm^3 and $a_4 = 0.7$ with $1.7\epsilon_n$, then $\epsilon_c = 4.56 \times 10^{14}$ g/cm^3 and therefore $P_c = 6.369 \times 10^{33}$ din/cm^2. On the other hand, if the central density is $3.3\epsilon_n$ then $P_c = 1.03114 \times 10^{35}$ din/cm^2. This shows that, as the central density is increased, the results obtained here are in agreement with the typical values of central pressures ($\approx 10^{35}$ din/cm^2) obtained for the strange star candidates presented in [48].

In summary, we have 100 values for the parameters $a_4^\perp$ and $B_\perp$ and 1000 values for the central energy density, so in total, we have performed to the order of 10^7 numerical simulations. The numerical simulations were carried out by using geometrized units; see Appendix.

IV. MASS-RADIUS RELATION OF AN ANISOTROPIC QUARK STAR

The mass-radius relation for spherically symmetric anisotropic quark star solutions was calculated for the case where the difference in the hydrostatic equation between the tangential and the radial pressure is nonzero. From Eqs. (1) and (4) the anisotropy occurs at the level of the tangential component of the pressure due to the spherical symmetry, so the radial composers a_4 and B are being fixed, while the tangential $a_4^\perp$ and $B_\perp$ are varied.

The first solution for the anisotropic quark star is displayed in Fig. 1 presenting the mass-radius relation where the bag constant is set to $B = 92$ MeV/fm^3. The parameters $a_4 = a_4^\perp = 0.7$ and $B_\perp$ take several values that cover a range among the isotropic solution [by taking the solutions of the Tolman-Oppenheimer-Volkoff equations given in Sec. II this reduces to the isotropic case when $(P - P_\perp) = 0$ in Eq. (8)], i.e., $B_\perp = 92$ MeV/fm^3, and the smallest value that the bag parameter can take, $B_\perp = 57$ MeV/fm^3. As it is expected, $B_\perp$ do not produce any significant effect with respect to the isotropic case and all the solutions are overlapped in a unique curve. Furthermore, these solutions fall in the gravitational waves observation range $1.17\ M_\odot < M < 1.6\ M_\odot$ [49] (green-blue region), and also in the upper limit mass $2.01\ M_\odot < M < 2.16\ M_\odot$ (beige region) recently found in [50].

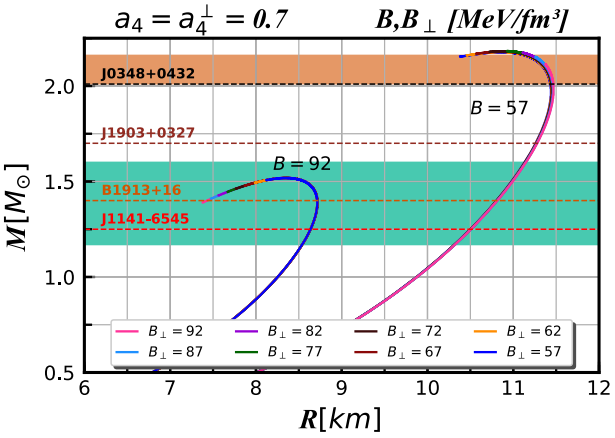

FIG. 1. Mass-radius relation for anisotropic quark stars with $a_4 = a_4^\perp = 0.7$.

In Fig. 2(a) the domain of solutions is around the static observational limit for neutron stars (beige region); although the solutions do not exhibit a monotonic behavior, the maximum mass of the solution with anisotropic factor $a_4^\perp = 0.2$ fits with the observational restriction on the static neutron star mass. One of the observational constraints on this matter was found in [51]. In this case, the mass of $(1.97 \pm 0.04)\ M_\odot$ for the pulsar $J1614 - 2230$ was determined through the Shapiro delay. On the other hand, the binary system composed by a white dwarf and the second pulsar $J0348 + 0432$ provided the most precise calculated mass of $(2.01 \pm 0.04)\ M_\odot$ [52]. Thus, this pulsar with a period of only 39.1226569017806(5) ms (or $f \approx 26$ Hz) has given one more $2\ M_\odot$ restriction, but also, the lower bound of the mass value for the static limit. As a result, it is possible to compare these pulsars and our results because their rotation frequencies are below the 300 Hz, which corresponds to the region where neutron stars are considered in the static limit regime [53].

By varying $a_4^\perp$ it is evident that the maximum mass and radius increase their values up to approximately 15% and 4.5%, respectively. This is a crucial result because it is possible to restrict the EOS for a fixed value of the bag parameter. Notice that similar results are achieved for the intermediate [see Fig. 2(b)] and upper limit [see Fig. 2(c)] of B. On the other hand, for $B = B_\perp = 77$ MeV/fm^3 the anisotropic parameter $a_4^\perp = 0.3$ (green solid line) fits with the observational mass for the pulsar $J1903 + 0327$; moreover, the increment of the mass is approximate to 12% and the radius is around a 4.2%. Meanwhile, for $B = B_\perp = 92$ MeV/fm^3, most of the solutions are found in the region corresponding to pulsars $J1903 + 0327$ and $J11441 - 6545$. Such masses are in agreement with estimations of gravitational waves from binary neutron star observations [49].

Likewise, the mass-central density relation is plotted in Fig. 3. It is evident that lowering the parameter $a_4^\perp$,

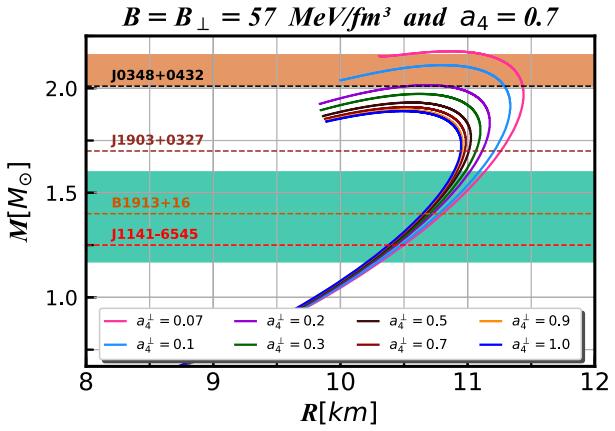

(a)

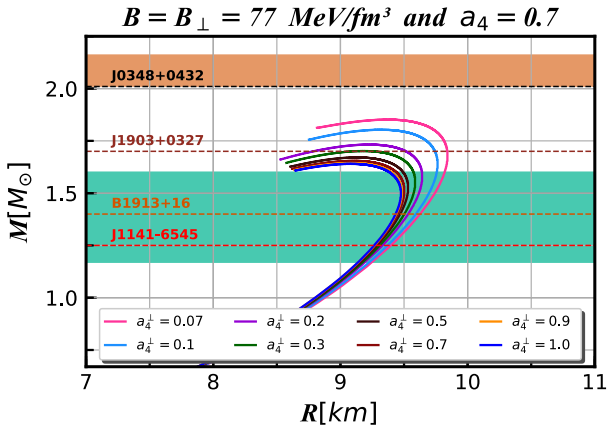

(b)

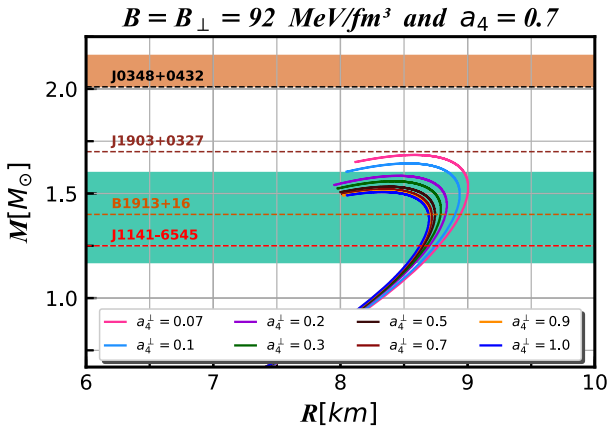

(c)

FIG. 2. Mass-radius curve for anisotropic quark stars for (a) $B_\perp = 57$, (b) $B_\perp = 77$, and (c) $B_\perp = 92$ MeV/fm^3: The mass constriction (beige region) [50] and the estimated mass from gravitational waves (green-blue region) [49], respectively.

the solutions tend to be more stable, even though they are not monotonically growing. In the same way, as the anisotropic factor is decreasing (i.e., the interactions between quarks become stronger) the system is more

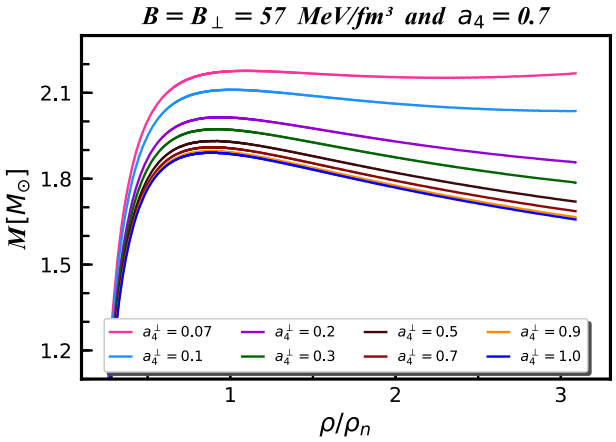

FIG. 3. Mass-density relation for the anisotropic quark star where $\rho_n = 2.4 \times 10^{14}$ g/cm^3.

stable. Notice that the stability is also influenced by the bag constant, in particular, for $B = B_\perp = 57$ MeV/fm^3 a saddle point seems to appear, although it does not happen for $B = B_\perp = 77$ MeV/fm^3 and $B = B_\perp = 92$ MeV/fm^3. In a word, the anisotropy stabilizes the quark star.

On the other hand, a profile of solutions that covers the full range of values for $a_4^\perp$ and $B_\perp$ is presented in Fig. 4. Although it is clear that B do not generate anisotropies, it has a significant influence on the maximum masses and radius, since the increment of $B = B_\perp$ contributes to the diminution of these two observables, similar to the outcomes obtained for the isotropic case (cyan dashed line). It is evident that for less interacting quarks the maximum masses and their corresponding maximum radius have larger values, but note that for highly interacting quarks the maximum masses do not even reach the 2 $M_\odot$ constraint. Equally important, there is a sector where the solutions never reach solutions with $a_4^\perp = 1.0$; in fact, for $B_\perp$ below 72 MeV/fm^3 there are no maximum masses that reach the noninteracting quark limit. Certainly, this may be considered a strong restriction for the EOS.

Another key point is the results obtained to roughly describe the interior of quark stars candidates taking into account the maximum mass and maximum radius observations (white solid lines). Due to this, it is possible to determine how much the quarks interact by restricting $B_\perp$, $a_4^\perp$, and a_4 for a given maximum mass and its corresponding radius. Nevertheless, it is not clear how the anisotropy mechanism is produced by $a_4^\perp$.

Finally, in Table I, we present some of the values of the maximum masses, the maximum energy densities, and their corresponding radii for some values of the parameters B, $B_\perp$, $a_4^\perp$ and a_4. Specifically, the presented values correspond to the case when the parameters B and $B_\perp$ are equal and the anisotropy is determined by the parameters $a_4^\perp$ and a_4.

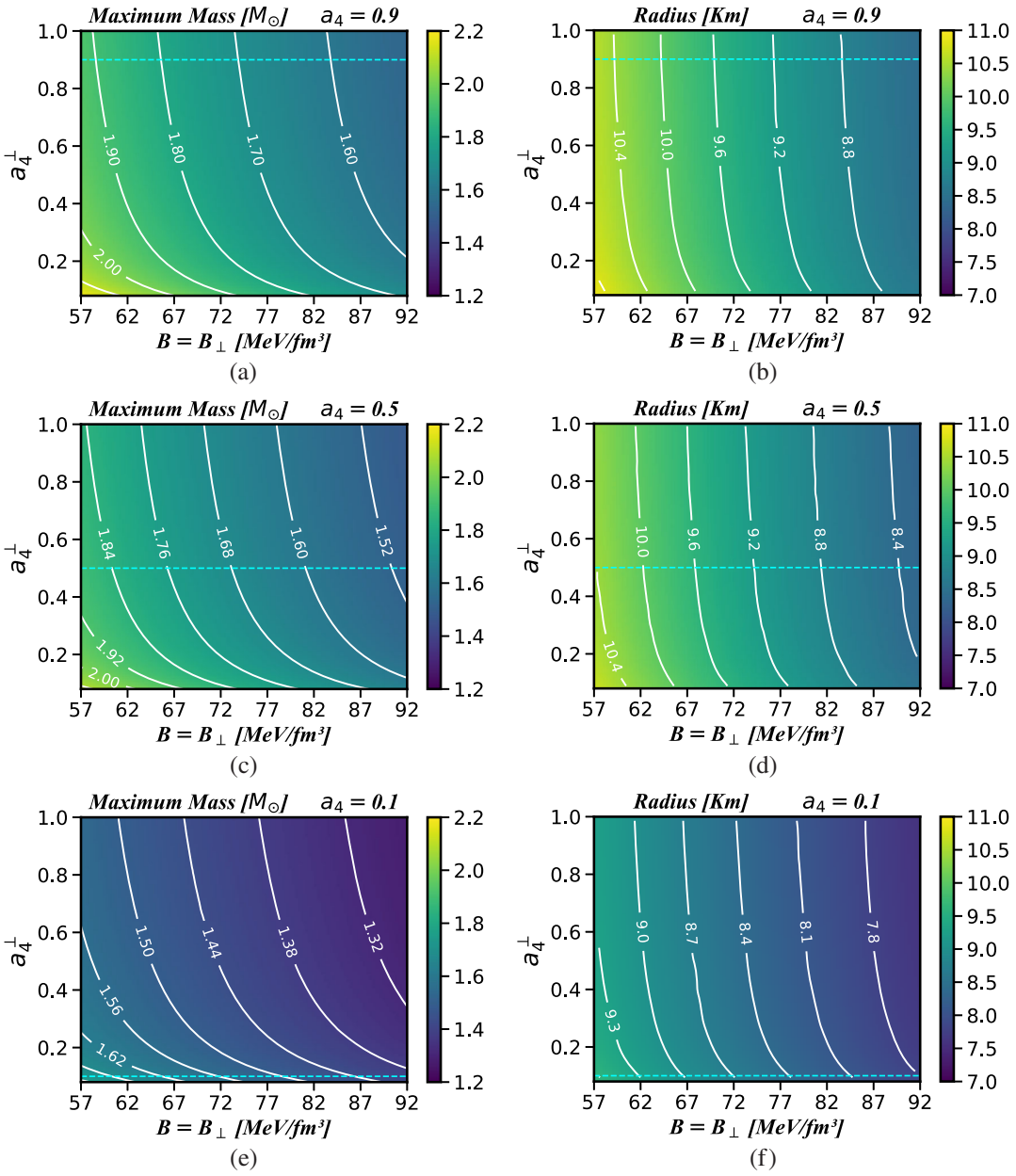

FIG. 4. Maximum masses and their corresponding radii for the full range of values of $a_4^{\perp}$ and $B_{\perp}$. The white lines are all QS in which the maximum mass and radius has the same value, and the cyan colored lines are the isotropic cases ($a_4 = a_4^{\perp}$).

V. BINDING ENERGY AND COMPACTNESS

At the quark star surface, the emission produced by the photons is calculated through the gravitational redshift [54]

$$Z_{\rm surf} = (1 - r_g/R)^{-1/2} - 1, \tag{10}$$

where $r_g = 2MG/c^2$, and R is the radius of the star.

A computation of the compactness leads to the redshift value for the isotropic case which is compared with the anisotropic solutions. Notice that the values of the gravitational redshift for the EOS [Eq. (4)] can be predicted. First, the isotropic and anisotropic maximum masses, and their corresponding radius, are used to calculate the redshift [Eq. (10)]. Since the compactness of $a_4 = 1.0$ and $a_4 = 0.7$ are similar, the redshift obtained for both cases is $Z_{\rm surf}^{a_4=1.0} = 0.462$ and $Z_{\rm surf}^{a_4=0.7} = 0.4643$, respectively. In contrast, $Z_{\rm surf}^{a_4=0.07} = 0.5641$ corresponds to the most interacting quark matter and consequently the most compact quark star modeled here. Then, this quantity is sketched for a particular value of the bag parameter and a fixed a_4 in Fig. 5, while the perpendicular contribution of the interacting term $a_4^{\perp}$ runs from 1.0 (blue solid line) to

TABLE I. Physical values of the maximum masses, the maximum energy densities, and their corresponding radii as a function of $B = B_\perp$, and different configurations of $a_4^\perp$ with fixed values of $a_4 = 0.1$, 0.5 and 0.9.

$B = B_\perp$ (MeV/fm^3)	a_4	$a_4^\perp$	$M_{\max}$ ($M_\odot$)	$R_{\max}$ (Km)	$\epsilon_{\max}$ (g/cm^3)
57	0.1	0.08	1.75	9.68	2.61×10^{15}
		0.20	1.64	9.49	2.46×10^{15}
		0.50	1.57	9.34	2.45×10^{15}
		1.00	1.54	9.28	2.41×10^{15}
77	0.5	0.08	1.80	9.24	3.26×10^{15}
		0.20	1.70	9.12	2.98×10^{15}
		0.50	1.64	9.04	2.86×10^{15}
		1.00	1.61	8.98	2.84×10^{15}
92	0.9	0.08	1.69	8.60	3.94×10^{15}
		0.20	1.60	8.51	3.53×10^{15}
		0.50	1.55	8.42	3.45×10^{15}
		1.00	1.53	8.42	3.24×10^{15}

0.07 (pink solid line). The comparison with respect to the isotropic case $a_4^\perp = 0.7$ (brown solid line) shows that the largest deviation of the compactness reaches up to a 14%. Additionally, we checked that the behavior of the compactness is essentially the same for all the allowed values of $B = B_\perp$; i.e., this decreases as long as the quarks are less confined.

On the other hand, the binding energy is explored for all the permitted values of the bag constant and the interacting parameter. It is evident from Fig. 6 that the binding energy is larger for the lowest bag parameter B and small values of anisotropic factor $a_4^\perp$. We have observed that the binding energy decreases monotonically, but also it is not linear from $a_4 = 0.9$ to $a_4 = 0.1$. Although the difference is not significantly large, the less interacting quarks have larger binding energy.

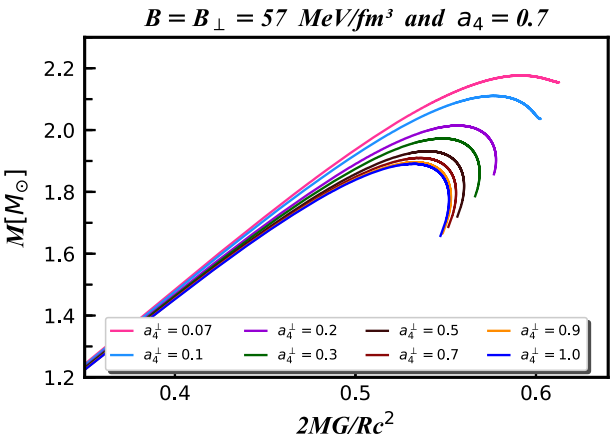

FIG. 5. Compactness $\mathcal{C}$ of anisotropic QS with $B = 57$.

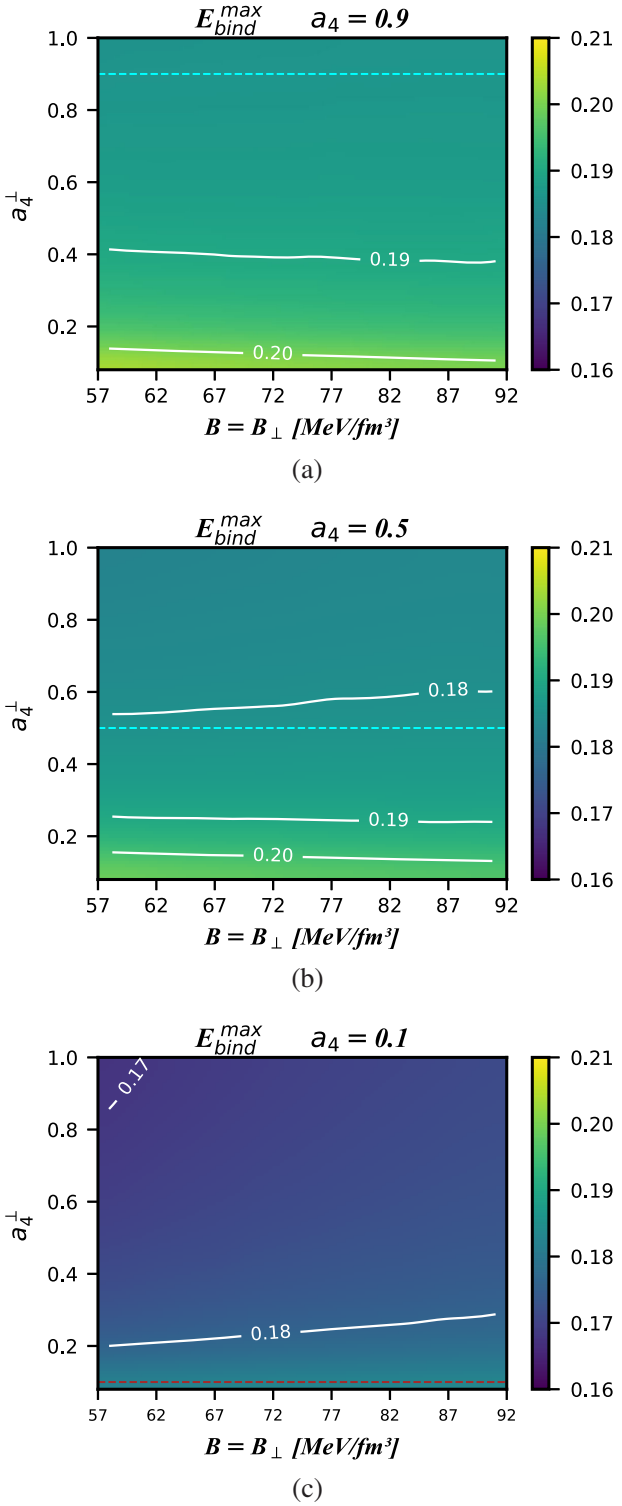

FIG. 6. Binding energy profile for the full set of solutions of the perpendicular component of the interacting parameter and the bag parameter.

VI. DISCUSSIONS AND CONCLUSIONS

From the EOS (1), it is clear that if the quark mass is 0, this reduces to the MIT bag model. On the other hand, the

corrections introduced by the coefficient a_4 produce similar results when there is no interaction among quark matter, but this is not clear at first sight due to the fact that a_4 [55] has a parametrization that depends on the corrections of the pressure of the free-quark Fermi sea. In consequence, this leads to the condition that if $a_4 = 1$, then matter is made of free noninteracting quarks. For values between $0 < a_4 < 1$ the quark interactions play a significant role because they can increase the neutron star mass up to three times and this can explain the importance of considering a strange or exotic matter EOS in the neutron stars cores, supporting the idea that quark stars may have masses ($0.7\ M_\odot$) smaller than those currently calculated for neutron stars [38]. Furthermore, the values of the interaction parameter that generate the observational constraint of $2\ M_\odot$ are over $a_4 = 0.5$, as it can be seen in the green-yellow region of Figs. 6(a) and 6(b).

Considering only the simple MIT bag model to study the anisotropy may be a naive approximation, since many models agree with the idea of the existence of the interacting matter in the strange and quark star interiors. Generally speaking, the value of $a_4^\perp$ is a parameter associated to the QCD of quark stars, but also is a cutoff of for their maximum and minimum masses. Therefore, these values can automatically restrict the quark star EOS through the anisotropy for a given B constrained by the range of energies at which it runs (57–92 $\mathrm{MeV/fm^3}$). In particular, Fig. 6(c) represents the changes that occur when $a_4 = 0.1$ is considered. Starting from the bottom of the plot, the binding energy along the isotropic line (dashed brown) that covers the values of the bag parameter from 57 to 92 $\mathrm{MeV/fm^3}$ is negligible. However, the anisotropy produced by the variation of $a_4^\perp$ generates small changes in the binding energy which are represented by the right-hand side column and whose values are shown explicitly on the plot (solid white lines) as isobinding energies. On the other hand, the binding energy associated to the bag parameter $B = 92\ \mathrm{MeV/fm^3}$ has some significant changes. In this case, the E_{bin} represented by the binding-energy isolines variate from ≈ 0.17 to ≈ 0.20 throughout the several solutions obtained for $a_4 = 0.1$, $a_4 = 0.5$ and $a_4 = 0.9$.

The results obtained above show that the effect of the bag parameter on the anisotropy is negligible; this may be due to the geometry of the stellar structure itself, because it is restricted to be spherically symmetric and any change on B does not affect this configuration. However, due to the interactions of the interior components of the quark stars being governed by the strong nuclear force, hence by the value of the interaction parameter, the major contribution to the anisotropy must come from $a_4^\perp$. As $a_4^\perp$ becomes larger the anisotropy produces less effect on the physical observables, since the quarks are almost free of interactions. However, for smaller values of $a_4^\perp$, the interaction among quarks becomes larger; in consequence, the anisotropy generates significant changes of up to 15% in the mass-radius relation.

ACKNOWLEDGMENTS

E. A. B.-V. acknowledges the financial support from COLCIENCIAS under the program Becas Doctorados Nacionales 727 and Universidad Industrial de Santander. S. M. acknowledges the support from the postdoctoral fellowship and Grants No. 2416 and No. 2314 provided by Universidad Industrial de Santander VIE-UIS. F. D. L.-C. was supported in part by VIE-UIS, under Grant No. 2493, by COLCIENCIAS, Colombia, under Grant No. 8863 and by Centro de Investigaciones-USTA under Grant No. 1952392. A. C. O. gratefully acknowledges the CONACYT postdoctoral fellowship (Grants No. 291168 and No. 291258). We thank L. Rezzolla for the useful discussion.

APPENDIX

In order to use the adequate units for the calculations presented here, we utilize geometrized units ($G = c = 1$) [56] for the parameters of the equation of the state. Starting with the expression that relates the geometrized pressure and the c.g.s. units

$$P_{cgs} = 5.55173 \times 10^{38} \left(\frac{M_\odot}{M}\right)^2 P_{geo},$$

and

$$1\ \frac{\mathrm{MeV}}{\mathrm{fm^3}} = 1.602176565 \times 10^{33}\, \frac{\mathrm{ergios}}{\mathrm{cm^3}}\,[=]\,\frac{\mathrm{din}}{\mathrm{cm^2}},$$

the conversion factor for the bag constant is given by

$$B_{geo} = \left(\frac{1.60218 \times 10^{33}}{5.55173 \times 10^{38}}\right) B_{[\mathrm{MeV/fm^3}]}.$$

Notice that the energy density ϵ has the same units as the bag constant. Additionally the mass of the quark strange is

$$m_{s_{geo}} = \left(\frac{1}{5.55173 \times 10^{38}}\right) m_{s_{cgs}}.$$

[1] K. Dev and M. Gleiser, Anisotropic stars: Exact solutions, Gen. Relativ. Gravit. **34**, 1793 (2002).
[2] M. K. Mak and T. Harko, Anisotropic stars in general relativity, Proc. R. Soc. A **459**, 393 (2003).
[3] F. E. Schunck and E. W. Mielke, General relativistic boson stars, Classical Quantum Gravity **20**, R301 (2003).
[4] C. Cattoen, T. Faber, and M. Visser, Gravastars must have anisotropic pressures, Classical Quantum Gravity **22**, 4189 (2005).
[5] H. Heintzmann and W. Hillebrandt, Neutron stars with an anisotropic equation of state—Mass, redshift and stability, Astron. Astrophys. **38**, 51 (1975).
[6] M. Ruderman, Pulsars: Structure and dynamics, Annu. Rev. Astron. Astrophys. **10**, 427 (1972).
[7] A. I. Sokolov, Phase transitions in a superfluid neutron liquid, JETP **52**, 575 (1980).
[8] B. Carter and D. Langlois, Relativistic models for superconducting-superfluid mixtures, Nucl. Phys. **B531**, 478 (1998).
[9] R. F. Sawyer, Bulk viscosity of hot neutron-star matter and the maximum rotation rates of neutron stars, Phys. Rev. D **39**, 3804 (1989).
[10] V. Canuto, Equation of state at ultrahigh densities, Annu. Rev. Astron. Astrophys. **12**, 167 (1974).
[11] V. Canuto, Neutron stars: General review, Ann. N.Y. Acad. Sci. **302**, 514 (1977).
[12] S. S. Yazadjiev, Relativistic models of magnetars: Non-perturbative analytical approach, Phys. Rev. D **85**, 044030 (2012).
[13] C. Y. Cardall, M. Prakash, and J. M. Lattimer, Effects of strong magnetic fields on neutron star structure, Astrophys. J. **554**, 322 (2001).
[14] L. Herrera and N. O. Santos, Local anisotropy in self-gravitating systems, Phys. Rep. **286**, 53 (1997).
[15] R. L. Bowers and E. P. T. Liang, Anisotropic spheres in general relativity, Astrophys. J. **188**, 657 (1974).
[16] M. Cosenza, L. Herrera, M. Esculpi, and L. Witten, Some models of anisotropic spheres in general relativity, J. Math. Phys. (N.Y.) **22**, 118 (1981).
[17] I. Bombaci, Observational evidence for strange matter in compact objects from the x-ray burster 4U 1820-30, Phys. Rev. C **55**, 1587 (1997).
[18] N. K. Glendenning, Prompt subsidence of a proto–neutron star into a black hole, Astrophys. J. **448**, 797 (1995).
[19] Z. Dai, Q. Peng, and T. Lu, The conversion of two-flavor to three-flavor quark matter in a Supernova core, Astrophys. J. **440**, 815 (1995).
[20] F. Rahaman, K. Chakraborty, P. Kuhfittig, G. C. Shit, and M. Rahman, A new deterministic model of strange stars, Eur. Phys. J. C **74**, 3126 (2014).
[21] K. S. Cheng, Z. G. Dai, and T. Lu, Strange stars and related astrophysical phenomena, Int. J. Mod. Phys. D **07**, 139 (1998).
[22] K. S. Cheng and Z. G. Dai, Are Soft γ-Ray Repeaters Strange Stars?, Phys. Rev. Lett. **80**, 18 (1998).
[23] A. Chodos, R. L. Jaffe, K. Johnson, C. B. Thorn, and V. F. Weisskopf, New extended model of hadrons, Phys. Rev. D **9**, 3471 (1974).
[24] E. Farhi and R. L. Jaffe, Strange matter, Phys. Rev. D **30**, 2379 (1984).
[25] M. K. Mak and T. Harko, An exact anisotropic quark star model, Chin. J. Astron. Astrophys. **2**, 248 (2002).
[26] H. A. Buchdahl, General relativistic fluid spheres, Phys. Rev. **116**, 1027 (1959).
[27] S. K. Maurya, Y. K. Gupta, S. Ray, and D. Deb, Generalised model for anisotropic compact stars, Eur. Phys. J. C **76**, 693 (2016).
[28] L. Herrera, Cracking of self-gravitating compact objects, Phys. Lett. A **165**, 206 (1992).
[29] D. Deb, S. Chowdhury, S. Ray, F. Rahaman, and B. Guha, Relativistic model for anisotropic strange stars, Ann. Phys. (Amsterdam) **387**, 239 (2017).
[30] D. Deb, S. Roy Chowdhury, S. Ray, and F. Rahaman, A new model for strange stars, Gen. Relativ. Gravit. **50**, 112 (2018).
[31] M. Rawls, J. Orosz, J. McClintock, M. Torres, C. Bailyn, and M. Buxton, Refined neutron star mass determinations for six eclipsing x-ray pulsar binaries, Astrophys. J. **730**, 25 (2011).
[32] T. Güver, F. Özel, A. Cabrera-Lavers, and P. Wroblewski, The distance, mass, and radius of the neutron star in 4U 1608-52, Astrophys. J. **712**, 964 (2010).
[33] P. C. C. Freire *et al.*, On the nature and evolution of the unique binary pulsar $J1903+0327$, Mon. Not. R. Astron. Soc. **412**, 2763 (2011).
[34] T. Güver, P. Wroblewski, L. Camarota, and F. Özel, The mass and radius of the neutron star in 4u 1820-30, Astrophys. J. **719**, 1807 (2010).
[35] P. B. Demorest, T. Pennucci, S. M. Ransom, M. S. E. Roberts, and J. W. T. Hessels, A two-solar-mass neutron star measured using Shapiro delay, Nature (London) **467**, 1081 (2010).
[36] X.-D. Li, Z.-G. Dai, and Z.-R. Wang, Is HER X-1 a strange star?, Astron. Astrophys. **303**, L1 (1995).
[37] X.-D. Li, I. Bombaci, M. Dey, J. Dey, and E. P. J. van den Heuvel, Is Sax j1808.4-3658 a Strange Star?, Phys. Rev. Lett. **83**, 3776 (1999).
[38] A. Schmitt, *Dense Matter in Compact Stars*, Lecture Notes in Physics Vol. 811 (Springer, Berlin, Heidelberg, 2010).
[39] P. Haensel, A. Potekhin, and D. Yakovlev, *Neutron Stars 1: Equation of State and Structure*, Astrophysics and Space Science Library Vol. 326 (Springer-Verlag, New York, 2007).
[40] C. V. Flores, Z. B. Hall, and P. Jaikumar, Nonradial oscillation modes of compact stars with a crust, Phys. Rev. C **96**, 065803 (2017).
[41] J. Asbell and P. Jaikumar, Oscillation modes of strange quark stars with a strangelet crust, J. Phys. Conf. Ser. **861**, 012029 (2017).
[42] J. Beringer *et al.*, Review of particle physics, Phys. Rev. D **86**, 010001 (2012).
[43] E. S. Fraga, R. D. Pisarski, and J. Schaffner-Bielich, Small, dense quark stars from perturbative QCD, Phys. Rev. D **63**, 121702 (2001).
[44] C. Misner, U. Misner, K. Thorne, J. Wheeler, and U. Thorne, *Gravitation, Science–Gravity* (W. H. Freeman, San Francisco, 1973).
[45] O. M. Pimentel, F. Lora-Clavijo, and G. A. González, The energy-momentum tensor for a dissipative fluid in general relativity, Gen. Relativ. Gravit. **48**, 124 (2016).

[46] F. D. Lora-Clavijo, A. Cruz-Osorio, and F. S. Guzmán, CAFE: A new relativistic MHD code, Astrophys. J. Suppl. Ser. **218**, 24 (2015).

[47] F. S. Guzman, F. D. Lora-Clavijo, and M. D. Morales, Revisiting spherically symmetric relativistic hydrodynamics, Rev. Mex. Fis. E **58**, 84 (2012).

[48] M. Kalam, A. A. Usmani, F. Rahaman, S. M. Hossein, I. Karar, and R. Sharma, A relativistic model for strange quark star, Int. J. Theor. Phys. **52**, 3319 (2013).

[49] B. P. Abbott *et al.* (LIGO Scientific and Virgo Collaborations), Gw170817: Observation of Gravitational Waves from a Binary Neutron Star Inspiral, Phys. Rev. Lett. **119**, 161101 (2017).

[50] L. Rezzolla, E. R. Most, and L. R. Weih, Using gravitational-wave observations and Quasi-universal relations to constrain the maximum mass of neutron stars, Astrophys. J. Lett. **852**, L25 (2018).

[51] P. Demorest, T. Pennucci, S. Ransom, M. Roberts, and J. Hessels, A two-solar-mass neutron star measured using shapiro delay, Nature (London) **467**, 1081 (2010).

[52] J. Antoniadis *et al.*, A massive pulsar in a compact relativistic binary, Science **340**, 1233232 (2013).

[53] F. Cipolletta, C. Cherubini, S. Filippi, J. A. Rueda, and R. Ruffini, Fast rotating neutron stars with realistic nuclear matter equation of state, Phys. Rev. D **92**, 023007 (2015).

[54] P. Haensel, A. Y. Potekhin, and D. G. Yakovlev, *Neutron Stars 1: Equation of State and Structure*, Astrophysics and Space Science Library Vol. 326 (Springer-Verlag, New York, 2007).

[55] M. Alford, M. Braby, M. Paris, and S. Reddy, Hybrid stars that masquerade as neutron stars, Astrophys. J. **629**, 969 (2005).

[56] L. Rezzolla and O. Zanotti, *Relativistic Hydrodynamics*, EBSCO ebook Academic Collection (Oxford University Press, Oxford, 2013).